Surface modification by nitrogen PIII on austenitic AISI 304 stainless steel

M. Castro-Colín[1], W. Durrer[2], J. A. López[2]* and E. Ramirez-Homs[2]

[1]Max Plank Institute für Intelligente Systeme, 70569 Stuttgart, Germany
Now at Bruker AXS GmbH, Karlsruhe, Germany
[2]Physics Department, University of Texas at El Paso, El Paso, TX 79968, USA

*Corresponding author: E-mail: jorgelopez@utep.edu

Resumen: Superficies de acero inoxidable AISI 304 nitrogenadas por tecnología PIII fueron estudiadas usando espectroscopía de electrones Auger (AES) y espectroscopía de foto-electrones emitidos por rayos X (XPS) para determinar el efecto de la nitrogenación en la superficie y capas subyacentes. La composición elemental obtenida por AES y XPS a varias profundidades indica que la concentración de Cr y O aumenta con la profundidad, la oxidación subyacente es producida por el barrido de Ar^+ usado para lograr acceso a las capas inferiores, y que el N está depositado en el Cr.

Abstract: Surfaces of AISI 304 austenitic stainless steel plates nitrided by PIII technology were studied by means of Auger electron spectroscopy (AES) and X-ray photoelectron spectroscopy (XPS) to determine the effect of the nitriding process on the surface and subjacent layers. Elemental compositions obtained by AES and XPS at varying depths indicate that the concentrations of both Cr and O increase with depth, that the subjacent oxidation is driven by the Ar^+ sputtering process used to access the lower layers, and that N is bound to Cr.

PACS 52.77.Dq, 68.49.Sf, 82.80.Ms, 79.60.-i

Keywords: PIII, AES, SIMS, nitriding, AISI 304 steel.

1. Introduction

Interest in plasma immersion ion implantation (PIII), as a technique for the treatment of industrial steels, is of great interest due to the advantageous modifications that it produces at the structural level. In particular, hardness and corrosion resistance (Anders, 2000) show improvement up to about 170% (López-Callejas, 2004).

Austenitic stainless steel is a wear and corrosion resistant type of steel. The austenitic phase is achieved typically by adding Ni, but also N can have a similar effect since it is an interstitial solute that can contribute to the formation of the face-centered-cubic austenitic phase. Nitrogen has an additional economic advantage over Ni, hence its importance. N also binds to Cr, competing with O, but at a lower rate, as seen later in the paper. The enthalpy of formation for CrN is -124.68 kJ mol^{-1} (Agouram 2004), less likely than either

Cr_2O_3 or CrO_2, with enthalpies of formation 1168.42 kJ mol-1, and -598 kJ/mol, (Kirklin 1999), respectively.

Nitrogen implantation of steel samples by plasma immersion at low temperatures (<300 ^oC) has shown to improve mechanical properties and corrosion performance (Tian et al., 2005; Tian and Chu, 2000). At higher temperatures control of corrosion through surface passivation due to interstitial nitrogen diffusion has been reported at ~400 ^oC (Mukherjee et al., 2002), while at temperatures >450 ^oC, the formation of CrN has been determined to reduce the anticorrosive properties of stainless steel (de Souza et al., 2004). Electrochemical corrosion properties have also been improved by nitriding through the PIII technique (Muñoz-Castro et al., 2005).

These studies point to the need of understanding the effect that PIII has on metallic surfaces, particularly those of austenitic stainless steel. We can add at this time that earlier studies (Langevoort *et al*., 1987) have shown that oxidation in AISI 304 can be measured starting at room temperature. Fe and Cr oxidize with equal rate up to 650 K, and >650K Cr oxidizes preferentially. Maintaining a Cr-oxidized surface layer in stainless steel is important due to its contribution to maintaining a protective layer that prevents Fe oxidation.

Several studies regarding structural improvements by plasma immersion technique have already been performed under different conditions. In a pioneering work, Zeng et al. (1999) employed ion implantation (Ti, Ta, Mo and W) of bearing steel samples immersed in a nitrogen plasma and used x-ray photoelectron spectroscopy (XPS) to study elemental depth profiles and chemical composition of the modified layers finding the formation of some nitride phases in the implanted layers. Years later, Zeng *et al*. (2004) performed argon and nitrogen PIII on gears of irregular shapes and used Rutherford backscattering spectrometry to discover large differences of implanted ion doses depending of the geometry of the surface. Other studies (Ueda et al., 2005) have used Auger electron spectroscopy (AES) and x-ray diffraction to characterize the effect that PIII has on the formation of chemical compounds in buried layers of metallic alloys.

In the present study we use AES and XPS to study austenitic steel AISI 304 exposed to a PIII nitriding process. The technique enables the analysis of the upper and particularly underlying buried layers down to about 52 and 86 nm after PIII nitriding.

2. Experimental setup

2.1 PIII treatment of steel samples

The PIII preparation of the steel samples used in this study has been reported with more detail elsewhere (López-Callejas et al., 2004). The samples used were made out of AISI 304 X5CrNi18-10 stainless steel of industrial grade (Metals Handbook, 1990) and had

dimensions of 20×20×3 mm. The samples were subjected to a nitrogen PIII process performed in the world smallest tokamac "Novillo" at Mexico's National Institute of Nuclear Research (Ramos et al., 1983). The toroidal chamber has inner and outer radii of 18 and 23 cm, respectively, and can have toroidal fields ranging from 0.05 to 0.47 T, plasma currents varying from 1 to 12 kA, electron densities within 1 to 2×10^{-13} cm^{-3}, and electron and ion temperatures of 150 and 50 eV, respectively. The implantation voltage used of –5 kV and had a pulse width ranged from 5 to 200 ms at a repetition frequency of 1 kHz. Each sample was immersed in the plasma for five hours.

In addition to the present study, the samples were also used to determine the electrochemical corrosion properties *in situ* as a function of the temperature, previously reported by López-Callejas and colleagues (Muñoz-Castro *et al.*, 2005). In the present study we focus on determining the effect of the PIII process on the elemental composition of the surfaces and subjacent layers of the steel samples through the use of AES and XPS studies.

2.2 AES and XPS parameters

AES was used to infer information on surface chemical composition and concentration. The surface characterization experiments were performed in a Perkin-Elmer PHI 560 ESCA/SAM system operating in an ultra-high vacuum (base pressure of 1×10^{-9} Torr) and containing multiple surface analytical techniques: AES, XPS and SIMS. Energy analysis for both the AES and XPS was accomplished using a Perkin-Elmer PHI model 25-270 AR double-pass cylindrical mirror analyzer (CMA). The instrument bombards the sample with a beam voltage of 2.0 kV with the filament energized to a standard emission setting of 0.6 mA, and an electron beam current of approximately 0.2 μA.

As explained by Davis and coworkers, the relative elemental concentration of the sample surface can be obtained by comparison against known compositions through the sensitivity of the system, which is determined from the collection efficiency of the analyzer, beam current and energy, and Auger transitions probabilities; sensitivity, scale factors, and Auger peaks can be found in reference (Davis et al., 1979). In our case the experimental errors arise from the difference in the system and the atomic work function, about 0.05%, or about 1 eV.

The XPS study was performed with the Perkin-Elmer PHI 32-095 X-ray source control with an aluminum anode (energy $h\nu$=1486.6 eV) energized to 200 Watts at 15 kV

2.4 Sputtering of samples

To study the nitrogen diffusion enabled by PIII into the sample, AES was performed on an internal layer in addition to the superficial one. The top layer was removed through argon ion bombardment at 3.0 kV over an area of 500×500 $microns^2$. The sputtering was

performed using the SIMS capability of the Perkin-Elmer PHI 560 ESCA/SAM. Argon sputtered the samples at 360 and 600 s while the chamber pressure was raised to 5×10^{-7} Torr, Fig. 1. AES was also carried out prior to any sputtering, Fig. 1.

3 Results and discussion

Figure 1 shows representative AES spectra obtained from the original surface (top curve) and of a buried layer (bottom curve), the latter at about 52 nm into the bulk. The AES spectra were obtained after 20 sweeps and collecting kinetic energy values in the range from 70 to 1070 eV in 5 eV bins.

Likewise, figure 2 illustrates the XPS results for the Cr (2p) and Fe (2p) regions using the customary inverse energy axis. The XPS spectra were obtained after 10 sweeps operating the Al anode at 200 W and 15 kV, and gathering binding energy in the range of 567 to 740 eV with bins of 0.5 eV to identify, among others, the Cr (2p), Fe (2p), and N (1s) peaks.

Altogether three different samples were studied as received (i.e. with the original surface) and after Ar^+ bombardment. Table 1 shows the results of the Auger analysis which reveal the presence of surface concentrations of S_1, C_1, N_1, O_1, Cr_2, and Fe_3 on all samples both with no Ar^+ beam sputtering (i.e. at zero seconds of bombardment) and after 360 or 600 seconds of exposure time, yielding depths of approximately 51.72 and 86.2 nm, respectively (Hofmann 1998; Hunt 1983). The elemental concentrations were obtained, as explained before, using AES. Note that the approach is valid because the AES collection time is the same in both cases, before and after sputtering.

Table 1: Elemental composition obtained from AES

	Sample 1		**Sample 2**		**Sample 3**	
Element	**0 s**	**360 s**	**0 s**	**600 s**	**0 s**	**600 s**
Fe_3	9.8 %	10.2 %	13.5 %	12.7 %	8.6.0 %	16.0 %
Cr_2	10.1 %	38.5 %	11.5 %	19.9 %	9.5 %	15.9 %
O_1	6.5 %	24.7 %	7.4 %	12.8 %	6.1 %	10.2 %
N_1	8.0 %	12.6 %	8.6 %	7.8 %	7.3 %	8.8 %
C_1	43.7 %	6.9 %	49.5 %	28.6 %	63.1 %	40.2 %
S_1	21.8 %	7.2 %	9.5 %	18.2 %	5.4 %	9.0 %

Typically (Stainless Steel, 2007) AISI 304 X5CrNi18-10 stainless steel is composed of C (<0.07 %), Mn (<2.00 %), Si (<1.00 %), Cr (17.5–19.5 %), Ni (8–10.5 %), P (<0.045 %), S (<0.015 %), N (<0.011 %) on a matrix of Fe (66–74 %). It is striking to detect N and O at large percentages both on the surface and in the deeper layers, particularly in the deeper layers, which would indicate a non-Fickian diffusion of both species.

3.1 Oxygen and iron

Before investigating the whereabouts of nitrogen, it is important to understand the unexpected behavior of oxygen. Figure 3 shows the concentrations of oxygen found before and after the Ar^+ sputtering. Clearly seen is the increase of O as a function of either sputtering or depth; percentagewise O increases by an average of 150%. For starters, the location of oxygen can be explained from the observed positions of XPS peaks for Fe, as seen in figure 2, the Fe (2p) peak occurs at an energy consistent with that of oxidized iron, possibly Fe_2O_3; although not shown in the figures, this situation occurs both on the original and buried surfaces in samples 1 and 2, although the Fe XPS peak of sample 3 probably corresponds to FeO.

The depth dependent increase of oxygen (Rhodes 2006) is the result of oxygen liberated via sputtering. Fe_2O_3 gets reduced with sputtering, and FeO gets formed in newly exposed layers since its enthalpy of formation is favourable compared to that of Fe_2O_3. The enthalpy of formation of chromium oxide also favors its formation; probably oxygen stripping during sputtering drives the protective oxidized chromium front, maintaining the corrosion resistance of the samples.

3.2 Nitrogen and chromium

Nitrogen absorbed during steelmaking results in interstitial solid solution strengthening which increases hardness. The relative percentage of nitrogen found by AES, however, appears to be much larger than expected from the production of the steel, which is of the order of hundredths of a percent.

Examining the table, nitrogen appears to maintain a percentage relatively constant as a function of depth. A possible explanation of this is provided by the XPS peaks of Cr which are consistent with those for less intensely oxidized Cr, possibly CrN for samples 1 (see Fig. 2) and 2, although for sample 3 the value corresponds probably to Cr_2S_3; Figure 4 shows the different components contributing to the XPS peak of Cr. The effect of the Ar^+ stripping on both Cr and N has also been reported before (Conde 2006) showing that the N peak in CrN increases with the sputtering while the Cr peak increases.

3.3 Oxygen and chromium

Obscured by the somewhat arbitrary AES percentages there exists an interesting relationship between Cr and O. Table 2 shows the previous data as a percentage growth

respect to the original value; in this manner, the percentage change of O of sample 1 is (24.7–6.5)/6.5×100 = 280%. Interestingly enough, Cr and O appear to have the exact same growths in percentage as measured with respect to the surface value.

Table 2: Growth of Cr_2 and O_1 relative to original percentages

Element	Sample 1 at 360 s	Sample 2 at 600 s	Sample 3 at 600 s
Cr_2	281.19 %	73.04 %	67.37 %
O_1	280.00 %	72.97 %	67.21 %

The identical increase could be explained by the fact that the main role of Cr in stainless steel is to form a passivation layer of chromium III oxide (Cr_2O_3) to improve the oxidation resistance of the steel; the interesting discovery is, however, that this oxidation persists and increases in the internal layers. This is explained by looking at the enthalpy of formation of Cr_2O_3, which is -1139 kJ/mol, smaller than that of Fe_2O_3, -824 kJ/mol. Thus, the oxygen released by sputtering, reacts with Fe and Cr, in a competing process. FeO is also susceptible of being formed, but its enthalpy of formation is -273 kJ/mol, diminishing its role in the competing oxidation process of the internal layers. The oxide peak of Fe (Wu 2004) is shown in Figure 5, but Fe_2O_3 and FeO are not indicated individually here. As expected the influence of carbon in the spectrum is observed in the Fe 2p peak, Fig. 5, actually making the largest area contribution

Another interesting feature is that carbon appears to have a larger percentage on the surface than on the internal layer. The role of carbon in steel is to form cementite (Fe_3C) which, in its orthorhombic lattice, presumably constitutes an easy target to the Ar ion. Texture analysis of the samples using X-ray diffraction, would permit to device a correlation between the carbon yield intensity and the relative content of the austenite and cementite phases. The latter studies have not been discussed here.

4 Conclusions

Surface studies of AISI 304 stainless steel plates subjected to nitrogen ion implantations by plasma immersion were carried out. Elemental compositions were obtained by AES and XPS at varying depths, 52 and 86 nm. The measurements indicate that the concentrations of both Cr and O increase with depth. The analysis indicates that the oxidation of Fe and Cr appears to be driven by the sputtering process itself, which also favors N binding to Cr, Fig. 5.

We would like thank R. López-Callejas (ININ) for providing the samples analyzed in this study and the participants of the VIII Symposium on Radiation Physics (April 9-11, 2012, IFUNAM, México DF, México) for interesting discussions.

References

Agouram, S., Bodart, F., and Terwagne, G., (2004) "LEEIX and XPS studies of reactive unbalanced magnetron sputtered chromium oxynitride thin films in air", *J. Electron Spectr. and Rel. Phenomena*, 134, 173-181.

ASM International Handbook Committee (1990) *Metals Handbook*, 10th Ed., vol. 1, ASM International, Materials Park, OH.

Anders, A. (2000) *Handbook of Plasma Immersion Ion Implantation and Deposition*, Wiley, New York, NY.

Conde, A., Cristobal, A.B., Fuentes, G., Tate, T., and de Damborenea, J., (2006) "Surface analysis of electrochemically stripped CrN coatings", *Surf. Coating Tech.* 201, 3588-3595.

Kirklin, D. R., (1999) "Properties of meterials and systems of importance to environmental fates and remediation III. Review of previous thermodynamic property values of chromium and some of its compounds", J. Phys. Chem. Ref. Data, 28 (6),

Davis, L.E., Macdonald, N.C., Palmberg, P.W., Riach, G.E. and Weber, R.E. (1979), Handbook of Auger Electron Spectroscopy, 2nd Ed., Perkin-Elmer Corporation.

De Souza, S.D., Olzon-Dionysio, M., Miola, E.J., and Paiva-Santos, C.O. (2004) "Plasma nitriding of sintered AISI 316L at several temperatures", *Surf. Coat. Technol*. 184 (2–3), p. 176.

Hofmann, S., (1998) "Sputtered depth profile analysis of interfaces", *Rep. Prog. Phys.* 61, 827-888

Hunt, C.P., and M. P. Seah, (1983) "Characterization of a high depth-resolution tantalum pentoxide sputter profile reference material", *Surf. Interface Anal.*, 5, 199.

Langevoort, J. C., Sutherland, I., Hanekamp, L. J., and Gellings, P. J. (1987) "On the oxide formation on Stailess Steels AISI 304 and Incoloy 800H investigated with XPS". *Appl. Surf. Sci.*, 28, 167-179.

López-Callejas, R., Valencia-Alvarado, R., Muñoz-Castro, A.E., Godoy-Cabrera, O.G., Barocio, S.R., and Chávez-Alarcón E., (2004) "Plasma immersion ion implantation of AISI 304 stainless steel in toroidal and cylindrical geometries", *Vacuum*, 76, 287–290.

Mukherjee, S., Chakraborty, J., Gupta, S., Raole, P.M., John, P.I., Rao, K.R.M., and Manna, I. (2002) "Low- and high-energy plasma immersion ion implantation for modification of material surfaces", *Surf. Coat. Technol.*, 156 (1–3), p. 103.

Muñoz-Castro, A.E., Valencia-Alvarado, R., Barocio, S.R., López-Callejas, R., Mercado-Cabrera, A., Godoy-Cabrera, O.G., Fuentes-González, D.A., and Arellano-Calderón, J. (2005), "Electrochemical corrosion properties of AISI 304 SS treated by low, intermediate and high temperature plasma immersion ionimplantation in a toroidal vessel", *Surface & Coatings Technology*, 200, 569– 572

Ramos, J., de Urquijo, J., Meléndez, L., Muñoz, A., Barocio S., Chávez, E., Balderas, E.G., Godinez, E., and Valencia, R. (1983), "Diseño del tokamac Novillo", *Rev. Mex. Fis.*, 29, 551-592.

Rhodes, K. R., (2006), "Sputter Reduction of Iron Oxide", *Mod. Microscopy J.*, http://www.modernmicroscopy.com/main.asp?article=71.

Stainless Steel: Tables of Technical Properties, 2nd Ed., (2007), *Materials and Application Series*, Vol. 5, Euro Inox 2007, Luxembourg.

Tian, X. and Chu, P.K. (2000) "Electrochemical corrosion properties of AISI304 steel treated by low-temperature plasma immersion ion implantation", *Scr. Mater.* 43, 417-422.

Tian, X.B., Wei, C.B., Yang, S.Q., Fu, R.K.Y. and Chu P.K. (2005), "Corrosion resistance improvement of magnesium alloy using nitrogen plasma ion implantation", *Surf. Coat. Technol.*, 198, 454-458

Ueda, M., Reuther H. and Lepienski, C.M. (2005), "Comparison of nitrogen ion beam and plasma immersion implantation in Al5052 alloy", *Nuc. Instr. Meth. Phys. Res. B: Beam Interactions with Materials and Atoms*, 240 (1-2), 199-203.

Wu, X, Cong, P., Nanao, H., Minami, I., and Mori, S., (2004) "Tribological behaviors of 52100 steel in carbon dioxide atmosphere", *Tribology Lett.*, 17, 4, 925-930.

Zeng, Z.M., Zhang, T., Tang, B.Y., Tian, X.B., and Chu P.K. (1999), "Surface modification of steel by metal plasma immersion ion implantation using vacuum arc plasma source", *Surf. Coat. Technol.*, 120-121, 659-662.

Zeng, Z. Fu, R.K.Y., Tian, X., and Chu P.K. (2004) "Plasma immersion ion implantation of industrial gears", *Surf. Coat. Technol.*, 186, 260-264.

Figures

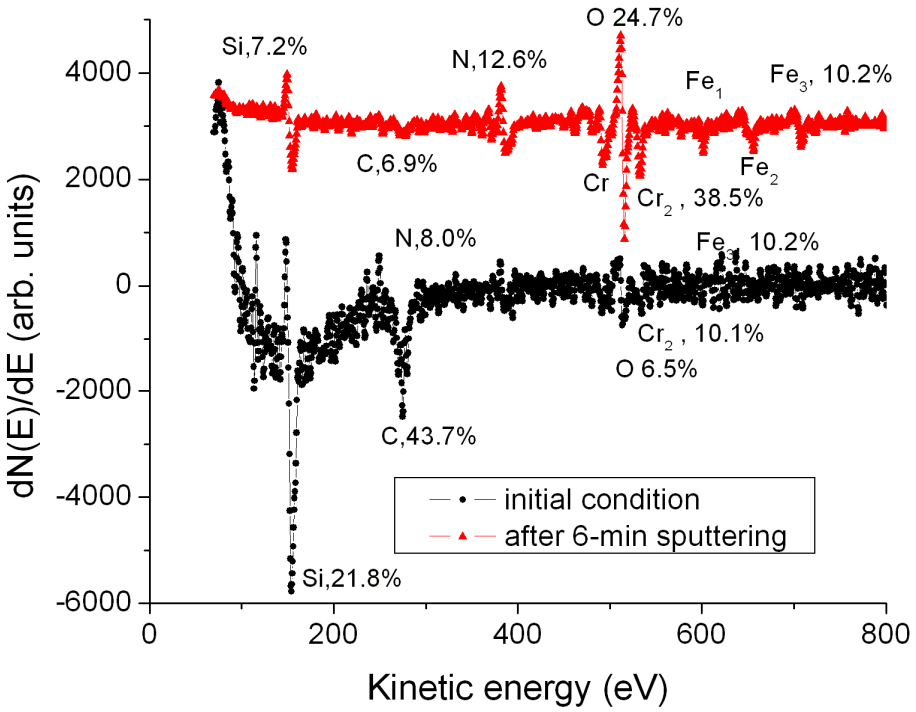

Figure 1. AES spectra of the sample in its initial condition (bottom) and after sputtering for six minutes down to 51.72 nm into the bulk (top).

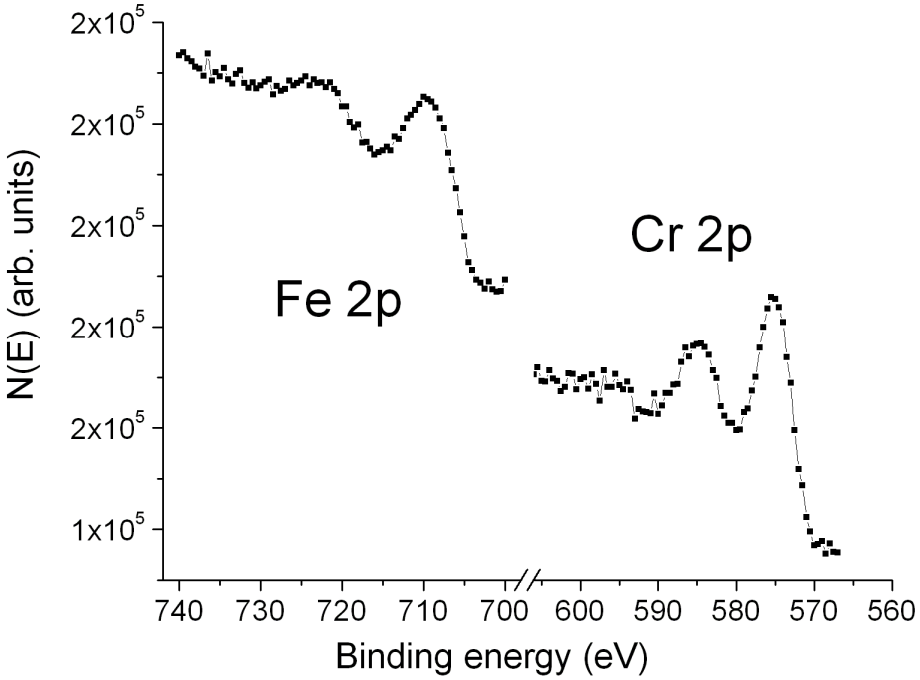

Figure 2. Characteristic Fe 2p and Cr 2p profiles obtained from the XPS spectra of the samples in its initial condition, i.e. before any sputtering.

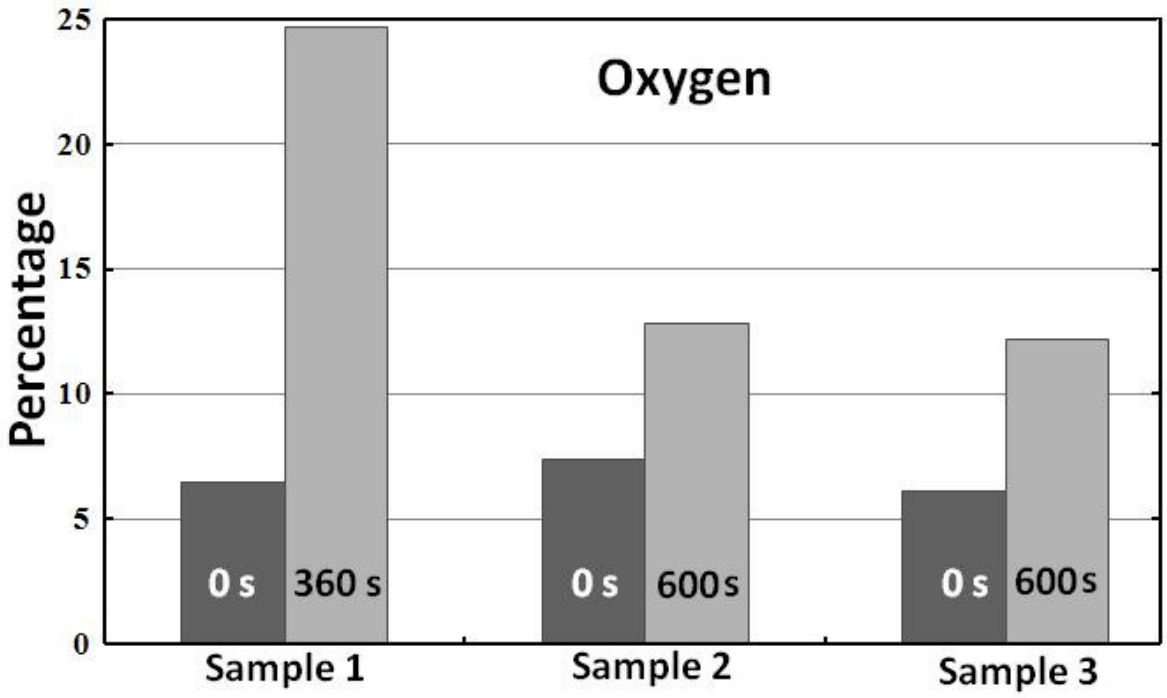

Figure 3. Concentrations of oxygen found in the three samples on the original surface (0 seconds of Ar^+ exposition) and after either 6 or 10 minutes of Ar^+ sputtering; the buried layers were estimated to be at 51.72 nm in sample 1 and 86.2 nm in samples 2 and 3.

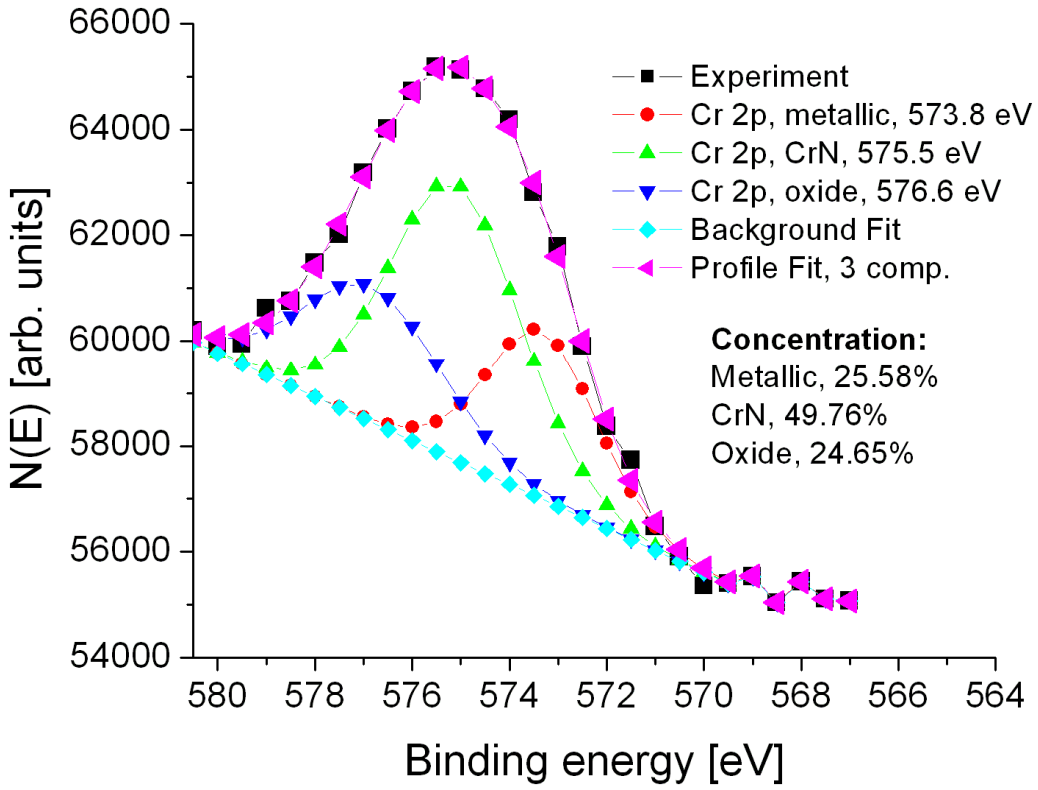

Figure 4. Fit of the XPS peak of Cr 2p and its components, elemental Cr, CN (predominantly) and oxidized Cr. The triangles correspond to the envelope of the three components.

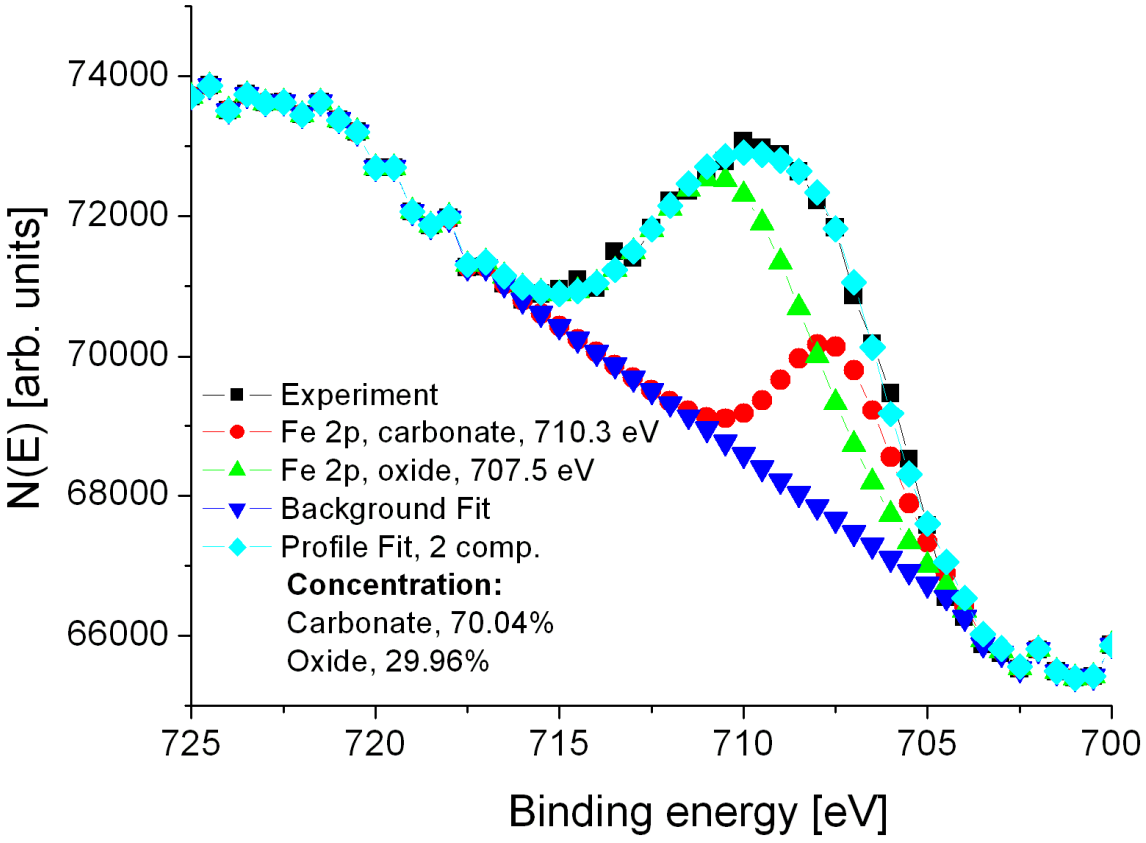

Figure 5. XPS peak of Fe 2p and its components, carbonate (triangles) and oxide (circles). The diamonds show the envelope obtained after the fit.